Interferometric tests of teleportation

T. C. Ralph*
Department of Physics, Centre for Lasers, The University of Queensland, St. Lucia 4072, Australia
(Received 20 December 2000; revised manuscript received 16 July 2001; published 13 December 2001)

We investigate a direct test of teleportation efficacy based on a Mach-Zehnder interferometer. The analysis is performed for continuous-variable teleportation of both discrete and continuous observables.

DOI: 10.1103/PhysRevA.65.012319 PACS number(s): 03.67.−a, 42.50.Dv, 42.50.−p

I. INTRODUCTION

Information is not independent of the physical laws used to store and process it [1]. The unique properties of quantum mechanics lead to radically different ways of communicating and processing information [2]. The study of ''quantum information'' is currently one of the fastest growing areas of physics.

Quantum teleportation [3–7] is a method by which quantum information can be passed through a classical channel and successfully retrieved at another location. The sharing of entanglement between the sender (Alice) and receiver (Bob) is essential for teleportation as it provides the ''quantum key'' needed to retrieve the quantum information [8]. In this way, an unknown quantum state of an object can be transferred through a classical channel, with neither Bob nor Alice knowing the state. As well as being a quantum communication tool, teleportation has also been identified as a quantum computational primitive [9]. Teleportation was originally described for discrete variables but now has been extended to continuous variables such as the quadrature amplitudes of optical fields [10].

The efficacy of teleportation can be characterized in a number of distinct ways. Traditionally fidelity is used for this purpose [11]. Fidelity, F, gives a measure of the quality of the teleported state by evaluating the overlap between the input state, $|\psi\rangle$, and the teleported output state, ρ, via $F=\langle\psi|\rho|\psi\rangle$. Fidelity is state-dependent, i.e., the fidelity of the reconstructed state depends both on the quality of the teleporter and on the class of input states from which the unknown state is picked.

For continuous-variable teleporters, criteria similar to those used to evaluate quantum nondemolition measurements have been proposed [12,13]. The most general of these is the amplitude conditional variance between the input and output beams [12,14]. The conditional variance measures the amount of uncorrelated noise that is added to the quantum state in the teleportation process. As such, it is a measure of the quality of the teleporter itself, independent of the state to be teleported. A continuous-variable teleporter introduces noise with Gaussian statistics, thus the conditional variance characterizes the added noise to all orders. Hence, once the conditional variance is known, the fidelity with which any state will be teleported can be calculated.

The measurement of either fidelity or the conditional variance involves a ''third'' person, Victor (the verifier), who prepares the input states and examines the teleported states to determine the quality of the teleportation. For example, Victor may prepare photons in particular polarization states and then check if they are still in the same states after teleportation [4,5]. For continuous-variable experiments, the signal and noise properties of the input and output are compared [7,15].

Another way of testing the efficacy of teleportation is to create a pair of quantum correlated objects, teleport one of them, then test directly to what extent they are still quantum correlated. An example of this is polarization entanglement swapping [6] in which one of an entangled pair of photons is teleported and then the degree of Bell entanglement that remains between them is determined by measuring the visibility of their photon correlations. The direct analog of this experiment using continuous-variable teleportation has also been proposed [16]. Tests based on the swapping of Einstein, Podolsky, and Rosen (EPR)-type entanglement have also been proposed [17,18]. Another possibility is to teleport one arm of a spatial superposition and then measure the preservation of the superposition directly through their interference characteristics. These types of tests are important for three reasons: (i) They directly observe the preservation of quantum correlations rather than just inferring them; (ii) such specific situations highlight aspects of the physics of the teleportation process not obvious from considering more general figures of merit; and (iii) from a practical point of view it would seem unlikely that teleportation could be successfully incorporated in any quantum information application unless interference and entanglement effects can be maintained above some threshold level.

A spatial superposition test can be applied to single photon polarization states using a Mach-Zehnder interferometer [19]. An interesting feature of such a test is that it is possible for Alice and Bob to verify that their teleporter is operating correctly without knowing the input states. In this paper, we generalize this test to cover a broad range of input states, including continuous-variable states. We will begin, in Sec. II, by introducing the model for a teleporter we will use throughout the paper. In Sec. III, we will review the operation of the Mach-Zehnder interferometer as a teleportation tester for single photon, polarization superposition inputs. Section IV will examine more general low photon number states and in Sec. V we will generalize the technique to input states with continuous degrees of freedom. In Sec. VI we will examine the relationship between our interferometric

*Email address: ralph@physics.uq.edu.au

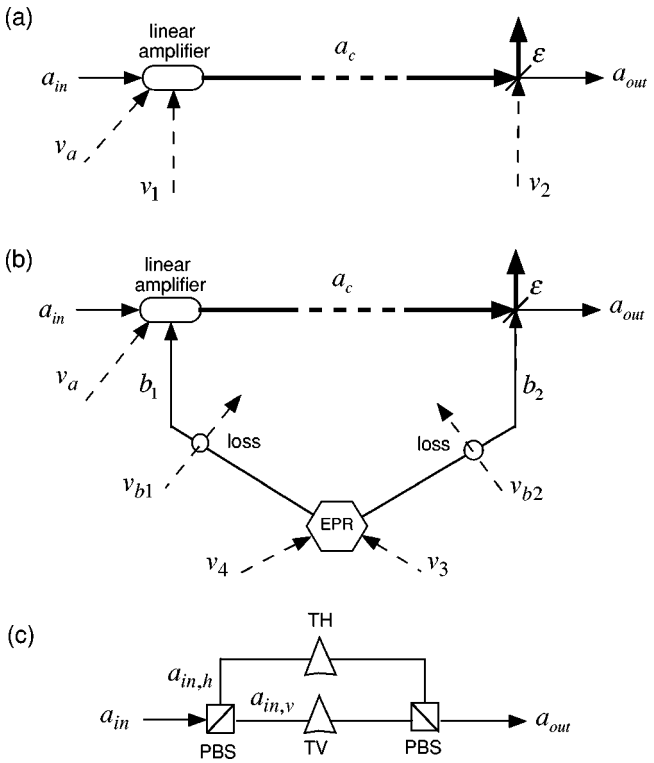

FIG. 1. Schematics of the all optical teleporter. In (a) a classical teleporter is shown (i.e., with no entanglement). In (b) the inclusion of entanglement (EPR) is shown. In (c) the separate teleportation of the two polarization modes is represented. TV and TH are the teleporters for the vertical and horizontal polarization components, respectively. PBS stands for polarizing beam splitter.

measure and the other teleportation measures. In Sec. VII we will discuss and conclude.

II. THE TELEPORTER

The teleporter we will consider in this paper is an all optical device using continuous-variable (squeezing) entanglement as a quantum resource [20]. This model is chosen for its versatility in being able to teleport all the input states considered in this paper. In an experimental situation, more input specialized devices may be used. Consider first the ''classical teleportation'' device depicted in Fig. 1(a). By classical we mean we attempt to transfer the quantum information through a classical channel without the assistance of entanglement. The input light field, $\hat{a}_{\rm in}(t)$, is sent through a linear optical amplifier by Alice. In Fourier space the output of a linear amplifier can be written as

$$a_c(\omega)=\sqrt{\eta_a G(\omega)}a_{\rm in}(\omega)+\sqrt{[G(\omega)-1]}v_1^\dagger + \sqrt{G(\omega)(1-\eta_a)}v_a, \tag{1}$$

where $G(\omega)$ is the (frequency-dependent) amplifier gain and v_1 and v_a are vacuum noise inputs due to the gain and internal losses (η_a) of the amplifier, respectively. If the gain is sufficiently large ($G\gg 1$) then a_c can be regarded as a classical field. This is because the conjugate quadrature variables $X_c^+=a_c+a_c^\dagger$ and $X_c^-=i(a_c-a_c^\dagger)$ both have uncertainties much greater than the quantum limit, i.e., $\Delta(X_c^\pm)^2\gg 1$. This means that simultaneous measurements of the conjugate quadratures can extract all the information carried by a_c with negligible penalty. The quantum noise added due to the simultaneous measurements will be negligible compared to the amplified quadrature uncertainties. It is thus possible to convert and then transmit the information carried in this beam over any available classical channel (radio, copper wires, etc.). However, it is convenient, and no less general, to retain an optical classical channel. Further discussion and a simple proof of the classical nature of this channel can be found in Appendix A.

When Bob receives the classical beam he attempts to retrieve the quantum state of the input by simply attenuating the beam with a beam splitter of transmission ε. The output field is $a_{\rm out}=\sqrt{\varepsilon}a_c-\sqrt{1-\varepsilon}v_2$, where v_2 is the vacuum mode incident on the unused port of the beam splitter. The final output field is thus

$$a_{\rm out}(\omega)=\lambda(\omega)a_{\rm in}(\omega)+\left(\frac{\lambda(\omega)}{\sqrt{\eta_a}}v_1^\dagger-v_2\right)+\lambda(\omega)\frac{\sqrt{1-\eta_a}}{\sqrt{\eta_a}}v_a, \tag{2}$$

where the total classical channel gain is given by $\lambda(\omega)=\sqrt{G(\omega)\varepsilon\eta_a}$ and we have assumed the classical channel limit $G\to\infty$ and $\varepsilon\to 0$. In practice, we are only interested in finite bandwidths. For photon counting experiments this usually means frequency filters will be placed in front of the detectors. For continuous-variable experiments only a finite range of RF frequencies will be analyzed. We will assume that the optical amplifier, and thus λ, has a flat response over the detection bandwidth. Hence, setting unity gain ($\lambda=1$) and negligible loss ($\eta_a=1$) we obtain the usual result

$$a_{\rm out}=a_{\rm in}+v_1^\dagger-v_2, \tag{3}$$

whereby two vacuum noise penalties are imposed by classical teleportation [10,12].

Quantum teleportation can be achieved by replacing the independent vacuum inputs, v_1 and v_2, with Einstein, Podolsky, and Rosen (EPR) entangled beams [21], b_1 and b_2, as shown in Fig. 1(b). Such beams have the very strong correlation property that both their difference amplitude quadrature variance, $\Delta(X_{b1}^+-X_{b2}^+)^2$, and their sum phase quadrature variance, $\Delta(X_{b1}^-+X_{b2}^-)^2$, are less than the quantum limit ($=1$). Such beams can be generated by subthreshold nondegenerate parametric amplification [21] or by the mixing of independent squeezed sources [22,12]. For nondegenerate parametric amplification these beams can be represented by

$$b_1(\omega)=\sqrt{\eta_{b1}H(\omega)}v_3+\sqrt{\eta_{b1}[H(\omega)-1]}v_4^\dagger+\sqrt{1-\eta_{b1}}v_{b1},$$
$$b2(\omega)=\eta b2H(\omega)v4+\eta b2[H(\omega)-1]v3\dagger+1-\eta b2vb2, \tag{4}$$

where $H(\omega)$ is the parametric gain and as before the η's and v's are efficiencies and resultant vacuum inputs, respectively.

The strength of the squeezing entanglement can be characterized by $V_{\rm ent}=(\sqrt{H}-\sqrt{H-1})^2$, which varies from not entangled ($V_{\rm ent}=1$) to strongly entangled ($V_{\rm ent}\to 0$) as the parametric gain increases. We will also refer to the percentage of entanglement squeezing as $(1-V_{\rm ent})\times 100\%$. The output field is now given by

$$a_{\rm out}(\omega)=\lambda(\omega)a_{\rm in}(\omega) + \left(\frac{\lambda(\omega)}{\sqrt{\eta_a}}b_1^{\dagger}(\omega)-b_2(\omega)\right)+\lambda(\omega)\frac{\sqrt{1-\eta_a}}{\sqrt{\eta_a}}v_a, \tag{5}$$

which, because of the strong correlations between b_1 and b_2, reduces to

$$a_{\rm out}(\omega)=\lambda(\omega)a_{\rm in}(\omega)+[\lambda(\omega)\sqrt{H(\omega)}-\sqrt{H(\omega)-1}]v_3^{\dagger} + [\sqrt{H(\omega)}-\lambda\sqrt{H(\omega)-1}]v_4 \tag{6}$$

in the absence of losses ($\eta_a=\eta_{b1}=\eta_{b2}=1$). Again we assume (and will do so for the remainder of the paper) that all gains are flat across the detection bandwidth. In the limit of very high parametric gain ($H\to\infty$, $V_{\rm ent}\to 0$) and unity classical channel gain ($\lambda=1$) the output becomes identical to the input ($a_{\rm out}\to a_{\rm in}$). This is ideal quantum teleportation as the only direct link between the input and output is the classical field a_c, yet arbitrarily accurate reconstruction of the input state is, in principle, possible with a sufficiently strong EPR correlation. The uncertainty principle is not compromised because the variances of each of the quadratures of b_1 by themselves are very noisy. Thus the information about $a_{\rm in}$ carried on the classical field is buried in this noise and cannot be extracted by using the classical field alone. An important operating point is the classical channel gain $\lambda_{\rm opt}=\sqrt{(H-1)}/\sqrt{H}$. With this gain, in the absence of losses, the output field is given by

$$a_{\rm out}=\lambda_{\rm opt}a_{\rm in}+(\sqrt{1-\lambda_{\rm opt}^2})v_4, \tag{7}$$

i.e., it is simply an attenuated version of the input [16]. The teleporter can be generalized to deal with arbitrary polarizations of the input field by decomposing the field into orthogonal polarization components (using a polarizing beamsplitter) and teleporting the individual components separately [see Fig. 1(c)].

The question remains as to how the linear amplifier in Fig. 1 could be constructed. This is not trivial as in standard optical amplifiers the source of the vacuum mode is not available for modification. For example, in a laser amplifier the physical origin of the vacuum input (v_1) is collisionally or phonon-induced dipole fluctuations of the gain medium [23]. One solution is shown schematically in Fig. 2. The input beam is mixed with the EPR beam, b_1, at a 50:50 beam splitter. The output beams are

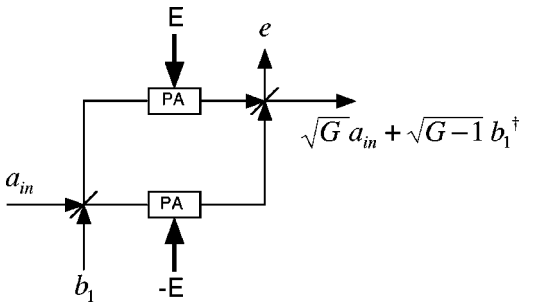

FIG. 2. Schematic of the linear amplifier used in the teleporters. The PA's stand for parametric amplifiers which are pumped in phase (E) and out of phase ($-E$) with the field.

$$c=\frac{1}{\sqrt{2}}(a_{\rm in}+b_1),$$

$$d=\frac{1}{\sqrt{2}}(a_{\rm in}-b_1). \tag{8}$$

The beams are amplified by degenerate parametric amplifiers of equal gains but with a π phase shift between their pump (E) phases. This results in the outputs

$$c'=\sqrt{G}c+\sqrt{G-1}c^{\dagger},$$

$$d'=\sqrt{G}d-\sqrt{G-1}d^{\dagger}. \tag{9}$$

Recombining these beams on a beamsplitter then produces the desired output: $a_c=\sqrt{G}a_{\rm in}+\sqrt{G-1}b_1^{\dagger}$.

III. THE MACH-ZEHNDER INTERFEROMETER AND THE TELEPORTER

We now examine the efficacy of the teleporter described in the previous section as characterized using an interferometer. In this section we will consider idealized single photon polarization superpositions as inputs to illustrate the basic physics. In the next section, we will consider more general polarization-number inputs. In the following section, continuous variable inputs will be considered.

Consider first the setup shown schematically in Fig. 3(a) [see also Fig. 4(a)]. Basically we place a teleporter in one arm of a Mach-Zehnder interferometer, inject a single photon state, in an arbitrary polarization superposition state into one port, then use the interference visibility at the output ports to characterize the efficacy of teleportation. A useful feature of this setup is that the visibility does not depend on the input state of the single photon, so we can assess how well the teleporter is working without knowing which particular polarization state is going into it. Let us see how this works.

The input for one port of the interferometer is in the arbitrary polarization superposition state

$$|\phi\rangle_a=x|1,0\rangle+y|0,1\rangle, \tag{10}$$

where $|n_h,n_v\rangle\equiv|n_h\rangle_h\otimes|n_v\rangle_v$, n_h and n_v are the photon numbers in the horizontal and vertical polarizations respec-

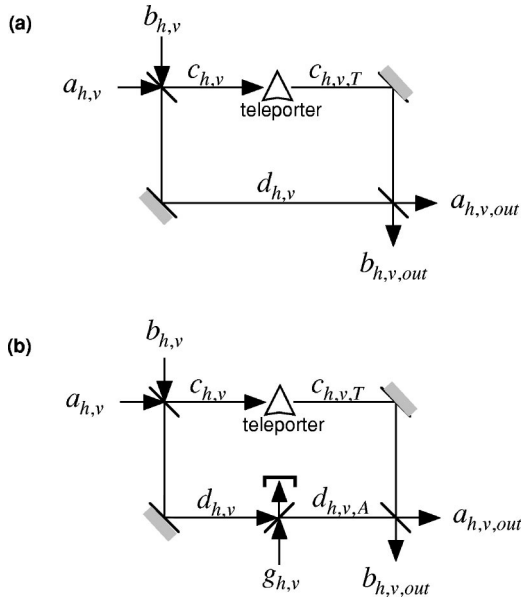

FIG. 3. Schematics of interferometric test arrangements.

tively, and $|x|^2+|y|^2=1$. The input of the other port is in the vacuum state $|\phi\rangle_b=|0,0\rangle$. The operators in the Heisenberg picture for the four input modes (two spatial times two polarization) are a_h and a_v (superposition) and b_h and b_v (vacuum). We propagate these operators through the Mach-Zehnder interferometer (including the teleporter). After the first beam splitter we can write

$$c_{h,v}=\frac{1}{\sqrt{2}}(a_{h,v}+b_{h,v}),$$
$$d_{h,v}=\frac{1}{\sqrt{2}}(a_{h,v}-b_{h,v}). \tag{11}$$

One of the beams (c) is then teleported. Under conditions for which losses can be neglected, we can use Eq. (6) to obtain

$$c_{h,v,T}=\lambda c_{h,v}+(\lambda\sqrt{H}-\sqrt{H-1})b^{\dagger}_{h,v,1}+(\sqrt{H}-\lambda\sqrt{H-1})b_{h,v,2}. \tag{12}$$

The fields are recombined in phase at the final beamsplitter giving the outputs

$$a_{h,v,\mathrm{out}}=\frac{1}{\sqrt{2}}(c_{h,v,T}+d_{h,v}),$$
$$b_{h,v,\mathrm{out}}=\frac{1}{\sqrt{2}}(c_{h,v,T}-d_{h,v}). \tag{13}$$

The expectation values for photon counting at the two outputs of the interferometer are

$$\begin{aligned}\langle a^{\dagger}_{\mathrm{out}}a_{\mathrm{out}}\rangle&=\langle\phi|_a\langle\phi|_b\langle\phi|_f(a_{h,\mathrm{out}}{}^{\dagger}+a_{v,\mathrm{out}}{}^{\dagger})\\&\quad\times(a_{h,\mathrm{out}}+a_{v,\mathrm{out}})|\phi\rangle_a|\phi\rangle_b|\phi\rangle_f\\&=0.25(1+\lambda)^2+(\lambda\sqrt{H}-\sqrt{H-1})^2,\\ \langle b^{\dagger}_{\mathrm{out}}b_{\mathrm{out}}\rangle&=\langle\phi|_a\langle\phi|_b\langle\phi|_f(b_{h,\mathrm{out}}{}^{\dagger}+b_{v,\mathrm{out}}{}^{\dagger})\\&\quad\times(b_{h,\mathrm{out}}+b_{v,\mathrm{out}})|\phi\rangle_a|\phi\rangle_b|\phi\rangle_f\\&=0.25(1-\lambda)^2+(\lambda\sqrt{H}-\sqrt{H-1})^2.\end{aligned} \tag{14}$$

In the limit of very strong entanglement squeezing ($V_{\mathrm{ent}}\rightarrow 0$), we find from Eq. (12) that $c_{h,v,T}\rightarrow c_{h,v}$ for unity gain ($\lambda=1$), i.e., perfect teleportation. For the same conditions (and only for these conditions) the visibility of the Mach-Zehnder outputs,

$$\mathcal{V}=\frac{\langle a^{\dagger}_{\mathrm{out}}a_{\mathrm{out}}\rangle-\langle b^{\dagger}_{\mathrm{out}}b_{\mathrm{out}}\rangle}{\langle a^{\dagger}_{\mathrm{out}}a_{\mathrm{out}}\rangle+\langle b^{\dagger}_{\mathrm{out}}b_{\mathrm{out}}\rangle}, \tag{15}$$

goes to 1, indicating the state of the teleported arm exactly matches that of the unteleported arm. Notice that the expectation values [Eq. (14)], and thus the visibility, do not depend on the actual input state (no dependence on x and y). Hence we can demonstrate that the teleporter is operating ideally even if we do not know the state of the input. Classical limits can be set by examining the visibility obtained with no entanglement ($H=1$). In Fig. 5, we plot the visibility versus feedforward gain in the teleporter for the cases of no entanglement (0%), 50% entanglement squeezing, and 90% entanglement squeezing. Maximum visibility occurs for the gain condition

$$\lambda=\frac{\sqrt{4H-3}}{\sqrt{4H+1}}, \tag{16}$$

giving $\mathcal{V}_{\max,c}=\sqrt{1/5}$ as the maximum visibility that can be obtained in the absence of entanglement. Increasing entanglement leads to increasing maximum visibility.

In the experiments we have imagined so far, the level of visibility has been determined not only by the ability of the teleporter to reproduce the input polarization states of the photons (the mode overlap), but also the efficiency with which input photons to the teleporter lead to correct output photons (the power balance). It is of interest to try to separate these effects. We can investigate just state reproduction if we allow attenuation to be applied to beam d, thus ''balancing'' the Mach-Zehnder interferometer by compensating for the loss introduced by the teleporter [see Fig. 3(b)]. The attenuated beam d becomes

$$d_{h,v,\mathrm{A}}=\sqrt{\eta}d_{h,v}+\sqrt{1-\eta}g_{h,v}, \tag{17}$$

where g is another vacuum field and η is the intensity transmission of the attenuator. The expectation values of the outputs are now

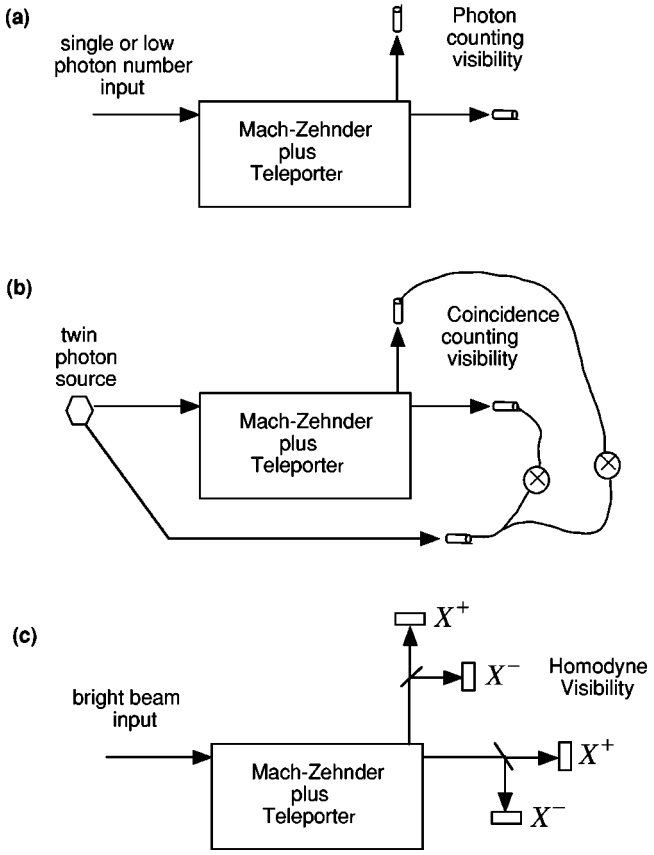

FIG. 4. Schematics of different input state-measurement techniques.

$$\langle a_{\rm out}^{\dagger} a_{\rm out}\rangle = 0.25(\sqrt{\eta}+\lambda)^2+(\lambda\sqrt{H}-\sqrt{H-1})^2,$$
$$\langle b_{\rm out}^{\dagger} b_{\rm out}\rangle = 0.25(\sqrt{\eta}-\lambda)^2+(\lambda\sqrt{H}-\sqrt{H-1})^2. \tag{18}$$

In Fig. 6, we plot visibility versus gain, using the attenuation η to optimize the visibility ($\eta \leqslant 1$). Now we can always achieve unit visibility for any finite level of entanglement by operating at gain,

$$\lambda_{\rm opt} = \sqrt{\frac{H-1}{H}} \tag{19}$$

and balancing the interferometer by setting $\eta = \lambda_{\rm opt}^2$. The high visibility is achieved because at gain $\lambda_{\rm opt}$ the teleporter behaves like pure attenuation [see Eq. (7)]. That is the photon flux of the teleported field is reduced, but no ''spurious photons'' are added to the field. Thus, at this gain, all output photons from the teleporter are in the right state, but various input photons are ''lost.''

This contrast between state-reproduction and efficiency has been a topic of vigorous debate [24,25]. It is of note that our interferometric test can separate the two effects. It should also be noted that our test is sensitive not only to the relative phase of the polarization superposition, but also the overall phase of the teleported field. The overall phase is defined with respect to the field in the unteleported arm of the interferometer and is a constituent of the mode overlap. If the overall phase is randomized by the teleporter then very low visibility will result from our interferometric test. At the end of Sec. IV, we will examine an interesting consequence of this additional sensitivity.

We now consider the effect of propagation loss in the two arms of the entangled source. Hence, referring back to Eq. (5), we set $\eta_{b1} = \eta_{b2} = \eta_b \neq 1$. We neglect for the moment the possibility of internal loss in the amplification (i.e., $\eta_a = 1$) or unequal loss in the two arms. With loss present (but not balancing the interferometer) the maximum visibility is achieved with the gain condition

$$\lambda_{\rm max} = \frac{\sqrt{4\eta_b(H-1)+1}}{\sqrt{4(1-\eta_b)+4\eta_b H+1}}. \tag{20}$$

In Fig. 7(a), we plot maximum visibility as a function of loss for various levels of entanglement squeezing. Visibility is reduced quite rapidly. If balancing of the interferometer is allowed, the gain condition for maximum visibility remains that found for no loss [Eq. (19)] but the balancing condition becomes $\eta = (5-4\eta_b)\lambda^2$. Once again, visibility drops off rapidly with increasing loss [see Fig. 7(b)] tending eventually to the classical limit as the loss completely wipes out the entanglement.

The effect of loss in the amplification (or measurement stage) ($\eta_a \neq 1$) produces very similar results to those in Fig. 7, as does indeed loss in only the entanglement arm sent to Alice (b_1). However, if loss is only present in the entanglement arm sent to Bob ($\eta_{b1} = 1, \eta_{b2} \neq 1$) things are rather different. The unbalanced visibility is still reduced with increasing loss but when the interferometer is balanced one can still achieve unit visibility by operating at the gain condition

$$\lambda_{\rm opt} = \frac{\sqrt{\eta_{b2}(H-1)}}{\sqrt{H}}. \tag{21}$$

Although the visibility is maintained, the efficiency is of course dropping. In the limit of strong loss, $\eta_{b2} \to 0$, the efficiency goes to zero and no photons are teleported.

IV. MORE GENERAL POLARIZATION INPUT STATES

So far we have assumed that the input state is a single photon number state. That is, there is unit probability that one, and only one, photon arrives per measurement interval. Such states are yet to be demonstrated experimentally, though candidate sources have been proposed [26–29]. However, the results of the previous section do not actually rely on the input being in a number state. An examination of Eq. (14) shows that it is only the *expectation value* of the photon number which is important. Thus any input state with an average photon number of one count per measurement interval will give identical visibilities to those of the previous section. An example is the low photon number coherent state $|\phi\rangle = |\alpha_h, \alpha_v\rangle$, in which $|\alpha_h|^2 + |\alpha_v|^2 = 1$. Such a state can approximately be produced by strongly attenuating a stable laser beam. We can generalize Eq. (14) for arbitrary average input photon number ($\bar{n}$) to obtain

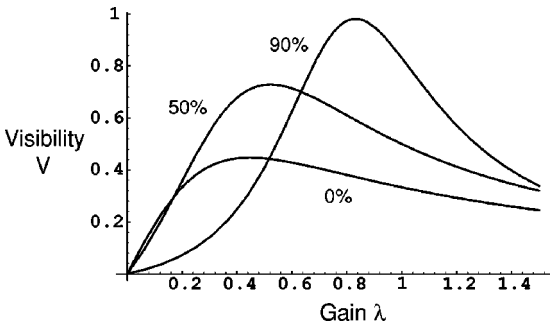

FIG. 5. Visibility versus gain for the setup shown in Fig. 3(a) and various levels of entanglement (0%, 50%, and 90%).

$$\langle a_{\rm out}^{\dagger}a_{\rm out}\rangle=\bar{n}0.25(1+\lambda)^2+(\lambda\sqrt{H}-\sqrt{H-1})^2,$$
$$\langle b_{\rm out}^{\dagger}b_{\rm out}\rangle=\bar{n}0.25(1-\lambda)^2+(\lambda\sqrt{H}-\sqrt{H-1})^2. \tag{22}$$

Maximum visibility now occurs for the gain condition

$$\lambda_{\rm max}=\frac{\sqrt{4H+\bar{n}-4}}{\sqrt{4H+\bar{n}},} \tag{23}$$

giving $\mathcal{V}_{\max,c}=\sqrt{\bar{n}/(\bar{n}+4)}$ for the maximum classical visibility. As might be expected, higher maximum visibilities can be achieved with only a classical channel as the average photon number increases and the input becomes more like a classical field. For average photon numbers less than 1, the maximum achievable visibility is reduced. This is basically a signal-to-noise effect. The penalty in classical teleportation arises from amplification of vacuum fluctuations (v_1) introduced in the ''measurement'' process. For low photon numbers this noise is large compared to the signal leading to low visibility. For large photon numbers the noise can become negligible compared to the signal leading to high visibilities. Figure 8 illustrates the change in $\lambda_{\rm max}$ and $V_{\rm max}$ as a function of entanglement for various values of the input photon number.

Single photon number states can be realized conditionally by using number entangled states. It is instructive to investigate this special case [see Fig. 4(b)]. A low efficiency, a

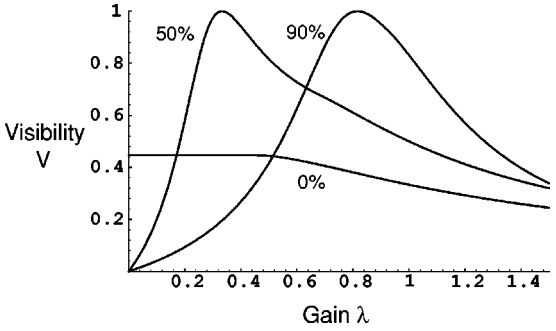

FIG. 6. Visibility versus gain with ''attenuation balancing'' [setup shown in Fig. 3(b)] for various levels of entanglement (0%, 50%, and 90%).

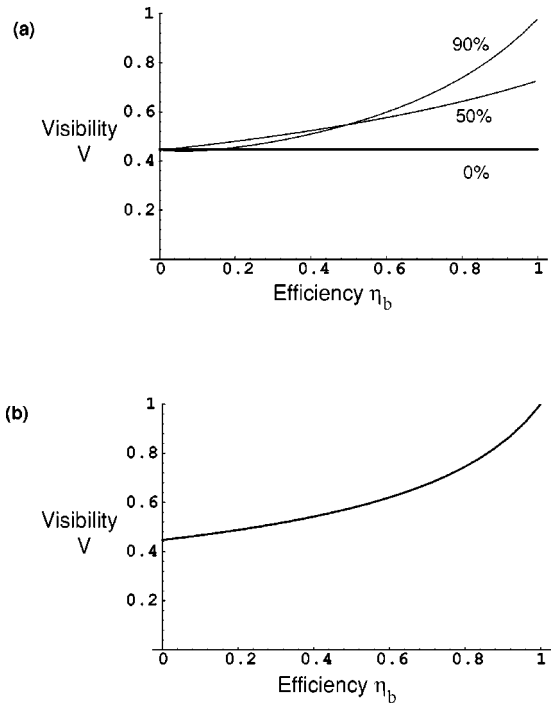

FIG. 7. The effect of loss on the visibility. In (a) the maximum visibility is plotted versus the transmission efficiency of the entangled beams for various levels of entanglement (0%, 50%, and 90%). In (b) balancing of the interferometer is allowed (plot is for 50% entanglement).

nondegenerate parametric amplifier (downconverter) can produce pairs of photons in the polarization-number entangled state

$$|\phi\rangle_{a,a'}\approx|0,0\rangle_a|0,0\rangle_{a'}+\chi(|1,0\rangle_a|1,0\rangle_{a'}+|0,1\rangle_a|0,1\rangle_{a'}), \tag{24}$$

where a and a' are the two, spatially separated fields and χ is the conversion efficiency. We have assumed $\chi\ll1$ and neglected higher-order terms in χ. As before, a is the input field to the interferometer plus teleporter and is transformed as per Eq. (13). We can either analyze the raw visibility of the outputs or the conditional visibility. Beam a by itself is in the unpolarized mixed state, given by the reduced density operator

$$\rho_a\approx|0,0\rangle\langle0,0|+\chi^2(|0,1\rangle\langle0,1|+|1,0\rangle\langle1,0|). \tag{25}$$

The raw count rates are thus calculated using $\langle a^{\dagger}a\rangle=\mathrm{Tr}[\rho a^{\dagger}a]$. As would be expected, the raw visibility is as predicted by Eq. (22) with $\bar{n}=\chi^2$. Because χ is small, classical teleportation visibilities will be low. However, with teleportation entanglement they can, in principle, reach unity. The relationship between interferometer visibilities and the fidelity of pure state teleportation will be discussed in Sec. VI. Here it is interesting to note that fidelity cannot be used to judge teleportation of the mixed state of Eq. (25). The fidelity between mixed input and output states is defined by [30]

$$F = \mathrm{Tr}[\sqrt{\rho_a^{1/2}\rho_{\mathrm{out}}\rho_a^{1/2}}]. \tag{26}$$

If $\rho_a = \rho_{\mathrm{out}}$, then $F = 1$. But this can easily be arranged by a cheating Alice and Bob without using entanglement. This is because *any* unpolarized mixed state with average photon number χ^2 will have a density operator equal to ρ_a. Only by making measurements of the joint state of a and a' before and after the teleporter and calculating a global fidelity can a high fidelity be considered proof of quantum teleportation. In contrast, a local interferometric test on only a unambiguously judges the quality of the teleporter. This is due to the sensitivity of the teleporter to the overall phase of the field. As a result, high visibilities are only possible when Alice and Bob share entanglement.

Conditional visibilities can be obtained by making the coincidence counts $\langle\phi|_{a,a'}\langle\phi|_b a'^{\dagger} a' a_{\mathrm{out}}^{\dagger} a_{\mathrm{out}}|\phi\rangle_b|\phi\rangle_{a,a'}$ and $\langle\phi|_{a,a'}\langle\phi|_b a'^{\dagger} a' b_{\mathrm{out}}^{\dagger} b_{\mathrm{out}}|\phi\rangle_b|\phi\rangle_{a,a'}$. Now counts are only recorded if a photon has simultaneously been detected in beam a'. This guarantees that only counts corresponding to times when a photon is launched into the interferometer are recorded. The visibilities then correspond to those obtained in Sec. II with single photon input states [31,32]. This result is conceptually different from the case of an average of one photon per measurement interval because it can be arranged, to a high probability, that only one photon is ever present at one time in the interferometer [33].

V. CONTINUOUS VARIABLE INPUTS

We now consider a very different type of input state and detection technique. Our input beam will now potentially be a ''bright'' beam. However, our interest will center only on the state of the ''side bands'' of the beam at some RF frequencies $\pm\omega$ around the central frequency. We will require that ω is sufficiently large that the power in the side bands at that frequency are of the order of one photon per second. Typically, for solid-state lasers, $\omega \rangle 10$ MHz will suffice. Instead of considering the polarization state of the light, as in the previous sections, we will now consider the field state of the side bands, as characterized by their distribution of power between phase and amplitude fluctuations. The total power in the side bands at the outputs can be measured using optical homodyne techniques and constructed visibilities. These visibilities behave identically to those in the photon counting case provided the average photon number in the side bands is equal to $\bar{n}$. This is quite surprising given the incompleteness of the formal analogy between single photon polarization states and single mode continuous variable states.

The proposed setup is shown in Fig. 4(c). It is identical to that for the single photon input except for the homodyne detection systems at the outputs instead of photon counters. The output beams are divided in half at beamsplitters and sent to homodyne detectors which detect orthogonal quadrature amplitudes, i.e.,

$$\begin{aligned} X^{+}(\omega) &= e^{i\theta} a(\omega) + e^{-i\theta} a^{\dagger}(\omega), \\ X^{-}(\omega) &= e^{i(\theta+\pi/2)} a(\omega) + e^{-i(\theta+\pi/2)} a^{\dagger}(\omega), \end{aligned} \tag{27}$$

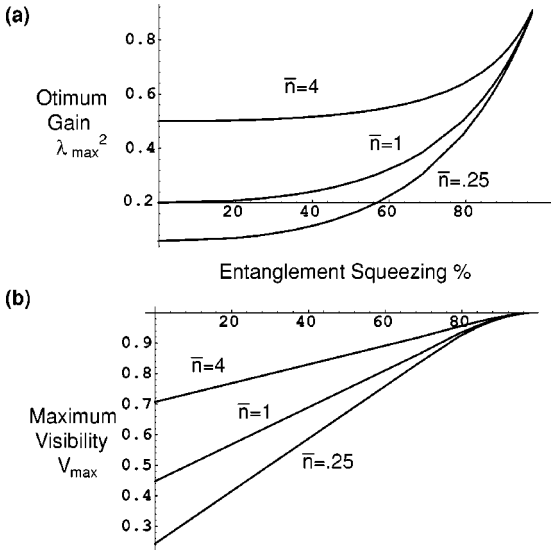

FIG. 8. Gain for maximum visibility (λ_{max}^2) and maximum visibility thus achieved (V_{max}) versus level of entanglement for various average input photon numbers ($\bar{n} = 0.25, 1.0, 4.0$).

where the absolute quadrature angle, θ, is arbitrary. Although the homodyne detection itself can be ideal, the splitting of the beams at the beamsplitters inevitably introduces vacuum noise (this must occur because orthogonal quadratures constitute conjugate observables). Thus the detection results are

$$\begin{aligned} X_a^{+}(\omega) &= \frac{1}{\sqrt{2}}[a_{\mathrm{out}}(\omega) + a_{\mathrm{out}}^{\dagger}(\omega) + v_{d1} + v_{d1}^{\dagger}], \\ X_a^{-}(\omega) &= \frac{i}{\sqrt{2}}[a_{\mathrm{out}}^{\dagger}(\omega) - a_{\mathrm{out}}(\omega) + v_{d1} - v_{d1}^{\dagger}], \\ X_b^{+}(\omega) &= \frac{1}{\sqrt{2}}[b_{\mathrm{out}}(\omega) + b_{\mathrm{out}}^{\dagger}(\omega) + v_{d2} + v_{d2}^{\dagger}], \\ X_b^{-}(\omega) &= \frac{i}{\sqrt{2}}[b_{\mathrm{out}}^{\dagger}(\omega) - b_{\mathrm{out}}(\omega) + v_{d2} - v_{d2}^{\dagger}], \end{aligned} \tag{28}$$

where the arbitrary angle θ has been set to zero for simplicity. The penalty vacuum noise is represented as usual by v's. Consider adding the photocurrents from each beam with a $\pi/2$ phase shift. This could be achieved by imposing a delay of τ to one of the currents such that $\tau\omega = \pi/2$. This gives photocurrents

$$\begin{aligned} A(\omega) &= X_a^{+} + iX_a^{-} = \sqrt{2}(a_{\mathrm{out}} + v_{d1}^{\dagger}), \\ B(\omega) &= X_b^{+} + iX_b^{-} = \sqrt{2}(b_{\mathrm{out}} + v_{d2}^{\dagger}). \end{aligned} \tag{29}$$

These photocurrents could then be fed into spectrum analyzers which give the photon number spectra

$$V_A(\omega)=\langle|X_a^+ + iX_a^-|^2\rangle = 2\langle a_{\rm out}^\dagger(\omega)a_{\rm out}(\omega)\rangle + 2,$$
$$V_B(\omega)=\langle|X_b^+ + iX_b^-|^2\rangle = 2\langle b_{\rm out}^\dagger(\omega)b_{\rm out}(\omega)\rangle + 2. \quad (30)$$

We can then define, in analogy with the photon counting case [Eq. (15)],the spectral visibility as

$$\mathcal{V}=\frac{\langle a_{\rm out}^\dagger(\omega)a_{\rm out}(\omega)\rangle - \langle b_{\rm out}^\dagger(\omega)b_{\rm out}(\omega)\rangle}{\langle a_{\rm out}^\dagger(\omega)a_{\rm out}(\omega)\rangle + \langle b_{\rm out}^\dagger(\omega)b_{\rm out}(\omega)\rangle} = \frac{V_A - V_B}{V_A + V_B - 4}. \quad (31)$$

Note that for an arbitrary field we can also write

$$\langle a_{\rm in}^\dagger(\omega)a_{\rm in}(\omega)\rangle = \langle \tfrac{1}{2}|X^+ + iX^-|^2\rangle = \tfrac{1}{4}(V^+ + V^-) - \tfrac{1}{2}, \quad (32)$$

where $V^+=\langle|X^+|^2\rangle$ and $V^-=\langle|X^-|^2\rangle$. Equation (32) allows us to construct visibilities directly from individually measured orthogonal quadrature spectral variances. Also it allows us to compare the visibilities obtained here with those of the previous sections. In order to make such comparisons with the photon counting visibilities, we observe that $\langle a_{\rm in}^\dagger(\omega)a_{\rm in}(\omega)\rangle$ is the photon number in the upper frequency component of the field only. Thus the total average photon number of upper and lower side bands (assuming a frequency-symmetric input state) is $\bar{n}(\pm\omega) = 2\langle a_{\rm in}^\dagger(\omega)a_{\rm in}(\omega)\rangle$. This is similar to the summing of the average photon numbers for both polarization modes in the discrete case. For equivalent average photon numbers [Eq. (22) with $\bar{n}(\pm\omega)\equiv\bar{n}$] *all* the predictions of the low photon number visibilities are exactly reproduced in the continuous variable case, including the ability to rebalance the interferometer and obtain unit visibilities.

The preceding analysis has shown that interferometric tests of quantum teleportation for unknown continuous variable states of a fixed average photon number can also be performed. Let us consider a couple of examples. For an arbitrary input field there will be some particular value of θ for which the conjugate spectral variances reach maximum and minimum values, $V_{\rm max}^+$ and $V_{\rm min}^-$, respectively. A minimum uncertainty state obeys the equality $V_{\rm max}^+ V_{\rm min}^- = 1$. It is convenient to discuss our examples in terms of these quadratures. Suppose our input field is quantum noise limited but with a small classical signal imposed at an arbitrary quadrature angle. This is equivalent to a coherent state of a particular amplitude but unknown phase. For this input $V_{\rm max}^+ = V_s + 1$ and $V_{\rm min}^- = 1$, where V_s is the signal power. If $V_s = 2$, then spectral visibilities identical to the single photon counting visibilities will be observed. Alternatively the input state may be squeezed at some arbitrary angle such that $V_{\rm max}^+ \rangle 1 \rangle V_{\rm min}^-$. If $V_{\rm max}^+ = 1/(2-\sqrt{3})$ and $V_{\rm min}^- = (2-\sqrt{3})$, then again spectral visibilities will be identical to the single photon counting visibilities.

These results are significant as reliable teleportation of spectral components is technologically less challenging than single photon experiments and are thus likely to form a significant part of future quantum information research.

VI. RELATIONSHIP TO OTHER MEASURES

We will now examine the relationship of the visibilities measured in our interferometric arrangement with the other measures for teleportation proposed and used in the literature. We will first derive a quite general direct relationship between the conditional variance of the teleporter and the measured visibility and then show by example how teleportation fidelities for particular input states can be calculated.

The amplitude conditional variance between the input and output of the teleporter is given by

$$V_{cv} = \frac{1}{2}[V_{\rm out}^+(1-C^+) + V_{\rm out}^-(1-C^-)], \quad (33)$$

where $V_{\rm out}^\pm = \langle|\delta X_{\rm out}^\pm|^2\rangle$ are the variances for the amplitude (δX^+) and phase (δX^-) quadrature fluctuations of the output state. The correlation function, C, is defined by

$$C^\pm = \frac{|\langle \delta X_{\rm in}^\pm \delta X_{\rm out}^\pm\rangle|^2}{V_{\rm in}^\pm V_{\rm out}^\pm}. \quad (34)$$

For the output field given by Eq. (5) we get

$$V_{cv} = \left(\lambda\sqrt{\frac{\eta_{b1}H}{\eta_a}} - \sqrt{\eta_{b2}(H-1)}\right)^2 + \frac{\lambda^2(1-\eta_{b1})}{\eta_a} + \left(\lambda\sqrt{\frac{\eta_{b1}(H-1)}{\eta_a}} - \sqrt{\eta_{b2}H}\right)^2 + (1-\eta_{b2}) + \frac{\lambda^2(1-\eta_a)}{\eta_a}. \quad (35)$$

Importantly this result is independent of the input field. From this result it can then be shown that in fact

$$V_{cv} = \frac{\lambda\bar{n}}{\mathcal{V}} + 1 - \lambda^2 - \frac{\bar{n}}{2}(1+\lambda^2). \quad (36)$$

Thus provided the gain of the teleporter (λ) and the average photon number of the input ($\bar{n}$) are known, then a measurement of the visibility immediately gives one a value for the conditional variance [34]. Although derived for the particular teleportation model of Sec. II, it can be shown that this result [Eq. (36)] is quite general, always applying provided: (i) the noise added by the teleporter is Gaussian and (ii) the gain of the teleporter is equal for both quadratures and is linear.

Once the conditional variance of the teleporter is known, then the fidelities that would be achieved when teleporting specific classes of states can be calculated. As a first example, consider a single photon number state, polarization qubits, as discussed in Sec. III. The teleportation fidelity can be calculated provided all the normally ordered moments of the output state are known (see Appendix B). It is straightforward to show that the normally ordered moments are given in terms of the conditional variance by

$$\langle a^{\dagger m}a^{m}\rangle=\left(\frac{1}{2}(V_{cv}+\lambda^{2}-1)\right)^{2m}m!+\left[m\lambda\left(\frac{1}{2}(V_{cv}+\lambda^{2}-1)\right)^{2(m-1)}\right](m-1)!. \tag{37}$$

In Fig. 9(a), we plot the visibility and inferred fidelity for single photon number states. Note that the fidelity is calculated for the situation where the qubits are teleported directly (not the case of the teleporter in the interferometer). We see that there is little apparent relationship between the two plots. However, it is standard in qubit teleportation experiments to disregard the efficiency of the teleporter and consider only the fidelity of state reconstruction when the teleportation is successful (i.e., conditional on the arrival of a photon) [4]. In Fig. 9(b), fidelity inferred in this way is compared with the visibility of a balanced interferometer. Now a relationship is seen with qualitatively similar behavior of the fidelity and visibility.

For our second example, we will consider the most experimentally relevant states for the short to medium term: continuous variable coherent states. Furusawa *et al.* [7] identified the boundary between classical and quantum teleportation of coherent states at a fidelity of 0.5. At about the same time we [12] concluded that a second, qualitatively different limit was given by a conditional variance of 1.0 at unity gain [35]. This second limit corresponds to a fidelity of 0.667. Since then, considerable evidence for the significance of this second limit has been presented in terms of the ability of the teleporter to reproduce quantum properties of the state [14,15], the quality requirements on the entanglement [14,13], and the uniqueness of the teleported state [13]. The existence of dual boundaries for entanglement-assisted phenomena is not unusual. For example, for discrete polarization entanglement the boundary for nonseparability is a coincidence visibility of 0.5 in all bases. On the other hand, violation of a Bell inequality requires visibilities greater than 0.71. Similarly, the requirements for violation of the continuous variable EPR condition [36] are more stringent than the nonseparability criterion for continuous variables [37].

The determination of these boundaries from the visibilities, measured as described in Sec. V, is straightforward. First, the visibility can be turned into a conditional variance using the relationship of Eq. (36). The fidelity that could be achieved with the teleporter can then be inferred using the relationship

$$F=\frac{2}{2+V_{cv}}\exp\left(-\frac{2|\alpha|^{2}(1-\lambda)^{2}}{2+V_{cv}}\right), \tag{38}$$

which can be derived from Ref. [7] with α the coherent amplitude of the input state. If the input states have unity average photon number, then the following correspondences apply at unity gain: a visibility of $\mathcal{V}=0.333$ corresponds to a conditional variance of $V_{cv}=2$ and infers a fidelity of $F=0.5$, while a visibility of $\mathcal{V}=0.5$ corresponds to a conditional variance of $V_{cv}=1.0$ and infers a fidelity of $F=0.667$.

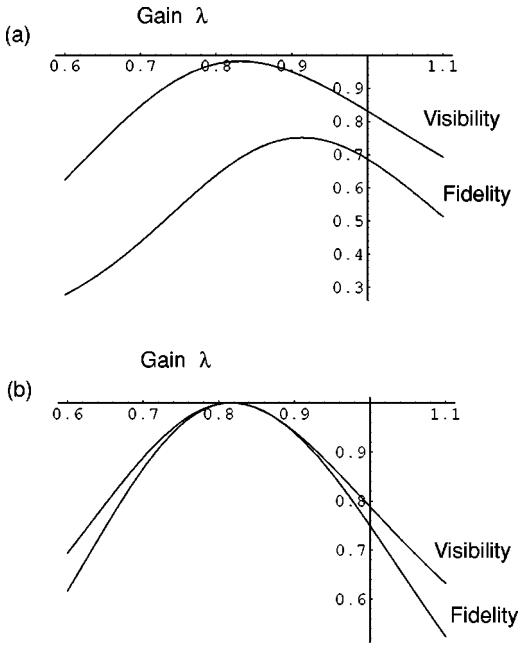

FIG. 9. Comparison of visibility of the interferometric test arrangement with fidelity which would be obtained in a standard teleportation experiment. Input state is a single photon polarization qubit. In (b) the results are corrected for efficiency by rebalancing the interferometer and calculating an efficiency-independent fidelity. No corrections are done in (a).

So far, continuous variable teleportation experiments have only explored the region close to unity gain. We have seen that the interferometric test highlights the interest of other gain conditions. In particular, with rebalancing very high visibilities may be obtained with finite entanglement squeezing. What is the significance of these visibilities? The conditional variance corresponding to substitution of the rebalanced visibility into Eq. (36) is an ''efficiency corrected'' conditional variance which depends on nonoptimal aspects of the protocol implementation, e.g., loss, but does not depend on the actual level of squeezing entanglement used. This could be a useful characterization. The fidelity that would then be inferred is an efficiency-corrected fidelity similar to that discussed for single qubits. In particular, we would infer

$$F_{\mathrm{corr}}=\langle\sqrt{\eta}\alpha|\rho|\sqrt{\eta}\alpha\rangle, \tag{39}$$

where η is the attenuation applied in rebalancing the interferometer. In other words, we infer the overlap that would be obtained between the output of the teleporter and an attenuated version of the input state.

VII. CONCLUSION

We have examined an interferometric test of the efficacy of teleportation. Unique characteristics of this arrangement are (i) it does not require the tester to know the input state of the light, only the average power; (ii) the ability of the tele-

porter to reconstruct both the relative and global phase of the field is tested directly; and (iii) one can directly test the state reconstruction ability of the teleporter separately from or together with its efficiency.

The teleportation efficacy is characterized by the visibility between the two outputs of a Mach-Zehnder interferometer when the teleporter to be tested is placed in one of the arms. We have contrasted the results obtained with no entanglement and varying levels of squeezing entanglement using continuous variable teleportation. A clear classical limit (i.e., with no entanglement) to the visibility was demonstrated and its dependence on input average photon number investigated. For an average photon count of one per measurement interval, the classical limit was $\mathcal{V} \leqslant \sqrt{1/5}$. Higher classical visibilities could be obtained with greater photon flux. The classical limit was lower with smaller photon flux. High visibilities (close to 1) could only be obtained (for low photon flux) with high levels of entanglement and low levels of loss. These are the requirements for high efficiency teleportation. However, decreased photon flux in the teleported arm (reduced efficiency) can be compensated by rebalancing the unteleported arm of the interferometer. In this way, state reconstruction can be tested separately from efficiency. We find that, provided losses are small, ideal state reconstruction can be achieved for any level of entanglement squeezing. This is characterized by unit visibility in the balanced interferometer with finite levels of entanglement. Losses reduce visibilities but the general trends remain the same.

A generalization of the technique to continuous variable inputs was presented. With suitable interpretation it was found that the visibilities exhibited identical behavior to their discrete variable counterparts.

We have discussed the relationship of the interferometric visibility to other figures of merit. Of considerable significance is the quite direct relationship between the visibility and the amplitude conditional variance of the teleporter. We showed by example how, once the value of the conditional variance had been obtained from visibility measurements, fidelities for arbitrary input states could be inferred.

We believe that tests of the kind outlined in this paper represent an important technique for characterizing quantum teleportation.

ACKNOWLEDGMENTS

We wish to thank A. G. White and G. J. Milburn for helpful discussions. This work was supported by the Australian Research Council.

APPENDIX A

Some readers may find it unusual that the classical channel a_c is described by an operator. This is a standard feature of the treatment of classical channels in the Heisenberg picture, *not* a consequence of our particular choice of an optical classical channel or our particular choice of teleporter model. The different treatments of classical channels between the Heisenberg and Schrödinger pictures are contrasted for quantum limited feedback in Ref. [38]. That a_c is truly a classical channel can be demonstrated easily via the no-cloning theorem [39], which states that a quantum system cannot be duplicated without penalty. If the quantum nature of a_c is significant in the teleportation process, then the no-cloning theorem would predict that duplication of a_c would lead to a significant degradation in the quality of the teleported state. An optimum continuous variable cloner can be constructed from the combination of a linear amplifier of gain 2 followed by a 50:50 beamsplitter. Applying this to a_c produces the two clones a_c' and a_c'' given by

$$\begin{aligned} a_c' &= a_c + \frac{1}{\sqrt{2}}(v_{c1}^\dagger + v_{c2}), \\ a_c'' &= a_c + \frac{1}{\sqrt{2}}(v_{c3}^\dagger - v_{c2}), \end{aligned} \tag{A1}$$

where the v's are vacuum modes. Suppose Bob uses a_c' for the reconstruction. He will produce the output

$$\begin{aligned} a_{\text{out}} = \lambda a_{\text{in}} + (\lambda\sqrt{H} - \sqrt{H-1})v_3^\dagger + (\sqrt{H} - \lambda\sqrt{H-1})v_4 \\ + \sqrt{\varepsilon}\,\frac{1}{\sqrt{2}}(v_{c1}^\dagger + v_{c2}). \end{aligned} \tag{A2}$$

The final term is due to the cloning process. But in the classical channel limit we have $\varepsilon \to 0$ and hence this final term can be neglected and Eq. (A2) reduces to Eq. (6). Arbitrarily good reconstruction of the input beam is still possible. The same result holds if Bob were to use the other clone, a_c'', for the reconstruction. Thus the cloning procedure does not change the quantum properties of the output and so a_c must be considered a classical channel.

APPENDIX B

The fidelity for a pure input state $|\sigma\rangle$ is given by

$$F_i = \langle \sigma | \rho_i | \sigma \rangle, \tag{B1}$$

where ρ_i is the density operator of the output state in the Schrödinger picture. First note that the action of the teleporter [as described by Eq. (13)] is independent of the polarization basis used to express it. That is, the Heisenberg equations will have identical form for any two orthogonal polarization modes. Thus the labels h and v can equally be interpreted as meaning horizontal and vertical or right and left circular, etc. This means we only need to evaluate the fidelity for some particular input polarization. The invariance with change of basis then implies that the same result will hold for all input polarizations. For simplicity, we choose horizontally polarized input photons such that $x=1$ and $y=0$. The fidelity then becomes

$$F_i = \langle 1|_h \langle 0|_v \rho_{i,h} \rho_{i,v} |0\rangle_v |1\rangle_h = \langle 1|\rho_{i,h}|1\rangle \langle 0|\rho_{i,v}|0\rangle, \tag{B2}$$

where the ouput density operator can be factorized into contributions from the two polarization modes, $\rho_i = \rho_{i,h}\rho_{i,v}$,

provided polarization cross-talk in the polarizing beamsplitters can be neglected. Thus the problem is reduced to finding the first and second diagonal elements of $\rho_{i,v}$ and $\rho_{i,h}$, respectively.

The diagonal elements of the density operator can be obtained from the normally ordered moments of the Heisenberg operators in the following way: suppose a Schrödinger picture density operator has the following general form:

$$\rho = p_0|0\rangle\langle 0| + p_1|1\rangle\langle 1| + p_2|2\rangle\langle 2| + \cdots p_n|n\rangle\langle n| + (\text{nondiagonal elements}), \tag{B3}$$

where we assume we can truncate at some sufficiently large photon number, n. The normally ordered moments are given by $\langle a^{\dagger m} a^m\rangle = \mathrm{Tr}\{a^{\dagger m} a^m \rho\}$ and are easily calculated from Eq. (B3) to be

$$\begin{aligned} \langle a^\dagger a\rangle &= p_1 + 2p_2 + 3p_3 + \cdots n p_n, \\ \langle a^{\dagger 2} a^2\rangle &= 2p_2 + 6p_3 + \cdots n(n-1)p_n, \\ \langle a^{\dagger 3} a^3\rangle &= 6p_3 + 24p_4 + \cdots n(n-1)(n-2)p_n, \\ &\cdots \\ \langle a^{\dagger n} a^n\rangle &= n! p_n. \end{aligned} \tag{B4}$$

From this result the following recursive relationship between the diagonal element probabilities and the moments can be obtained:

$$\begin{aligned} p_n &= \frac{1}{n!}\langle a^{\dagger n} a^n\rangle, \\ p_{n-1} &= \frac{1}{(n-1)!}\left(\langle a^{\dagger n-1} a^{n-1}\rangle - \frac{n!}{1!}p_n\right), \\ p_{n-2} &= \frac{1}{(n-2)!}\left(\langle a^{\dagger n} a^n\rangle - \frac{(n-1)!}{1!}p_{n-1} - \frac{n!}{2!}p_n\right), \\ &\cdots \\ p_1 &= (\langle a^\dagger a\rangle - 2p_2 - 3p_3 - \cdots n p_n, \\ p_0 &= 1 - p_1 - p_2 - p_3 - \cdots p_n. \end{aligned} \tag{B5}$$

Of course the operator moments are equivalent whether calculated in the Schrödinger or Heisenberg pictures. Calculation of the various moments in the Heisenberg picture proceeds as described in Sec. VI. Substitution into the general formula given by Eq. (B5) allows us to numerically calculate the required coefficients.

[1] R. Landauer, Phys. Today **23**, 5 (1991).
[2] C. H. Bennett and D. P. DiVincenzo, Nature (London) **404**, 247 (2000).
[3] C. H. Bennett, G. Brassard, C. Crepeau, R. Jozsa, A. Peres, and W. K. Wootters, Phys. Rev. Lett. **70**, 1895 (1993).
[4] D. Bouwmeester, J-W. Pan, K. Mattle, M. Eibl, H. Weinfurter, and A. Zeilinger, Nature (London) **390**, 575 (1997).
[5] D. Boschi, S. Branca, F. De. Martini, L. Hardy, and S. Popescu, Phys. Rev. Lett. **80**, 1121 (1998).
[6] Jian-Wei Pan, Dik Bouwmeester, Harald Weinfurter, and Anton Zeilinger, Phys. Rev. Lett. **80**, 3891 (1998).
[7] A. Furusawa, J. L. Sorensen, S. L. Braunstein, C. A. Fuchs, H. J. Kimble, and E. S. Polzik, Science **282**, 706 (1998).
[8] D. Deutsch and P. Hayden, Proc. R. Soc. London, Ser. A **456**, 1759 (2000).
[9] D. Gottesman and I. L. Chuang, Nature (London) **402**, 390 (1999).
[10] S. L. Braunstein and H. J. Kimble, Phys. Rev. Lett. **80**, 869 (1998).
[11] B. Schumacher, Phys. Rev. A **51**, 2738 (1995).
[12] T. C. Ralph and P. K. Lam, Phys. Rev. Lett. **81**, 5668 (1998).
[13] F. Grosshans and P. Grangier, Phys. Rev. A **64**, 010 301(R) (2001).
[14] T. C. Ralph, *Directions in Quantum Optics*, edited by H. J. Carmichael, R. J. Glauber, and M. O. Scully (Springer-Verlag, Berlin, 2001), p. 187.
[15] T. C. Ralph, P. K. Lam, and R. E. S. Polkinghorne, J. Opt. B: Quantum Semiclassical Opt. **1**, 483 (1999).
[16] R. E. S. Polkinghorne and T. C. Ralph, Phys. Rev. Lett. **83**, 2095 (1999).
[17] S. M. Tan, Phys. Rev. A **60**, 2752 (1999).
[18] P. van Loock and Samuel L. Braunstein, Phys. Rev. Lett. **84**, 3482 (2000).
[19] T. C. Ralph, Phys. Rev. A **61**, 044301 (2000).
[20] T. C. Ralph, Opt. Lett. **24**, 348 (1999).
[21] Z. Y. Ou, S. F. Pereira, H. J. Kimble, and K. C. Peng, Phys. Rev. Lett. **68**, 3663 (1992).
[22] G. Yeoman and S. M. Barnett, J. Mod. Opt. **40**, 1497 (1993).
[23] Y. Yamamoto, S. Machida, and O. Nilsson, Phys. Rev. A **34**, 4025 (1986).
[24] S. L. Braunstein and H. J. Kimble, Nature (London) **394**, 840 (1998).
[25] D. Bouwmeester, J-W. Pan, H. Weinfurter, and A. Zeilinger, J. Mod. Opt. **47**, 279 (2000).
[26] J. Kim, O. Benson, H. Kan, and Y. Yamamoto, Nature (London) **397**, 500 (1999).
[27] C. L. Foden, *et al.*, Phys. Rev. A **62**, 011803 (2000).
[28] B. Lounis and W. E. Moerner, Nature (London) **407**, 491 (2000).
[29] Christian Kurtsiefer, *et al.*, Phys. Rev. Lett. **85**, 290 (2000).
[30] H. Barnum, C. M. Caves, C. A. Fuchs, R. Jozsa, and B. Schumacher, Phys. Rev. Lett. **76**, 2818 (1996).
[31] C. K. Hong and L. Mandel, Phys. Rev. Lett. **56**, 58 (1986).
[32] A. I. Lvovsky *et al.*, Phys. Rev. Lett. **87**, 050402 (2001).
[33] P. Grangier, G. Roger, and A. Aspect, Europhys. Lett. **1**, 173 (1986).

[34] The fact that interferometric visibility directly relates to added noise (as the conditional variance measures) has been used previously to characterize amplifier quantum noise in R. C. Swanson, P. R. Battle, and J. L. Carlsten, Phys. Rev. A **45**, 1932 (1992).
[35] This point corresponds to the origin of the T-V graph of Ref. [12].
[36] M. D. Reid and P. D. Drummond, Phys. Rev. Lett. **60**, 2731 (1988).
[37] L-M. Duan, G. Giedke, J. I. Cirac, and P. Zoller, Phys. Rev. Lett. **84**, 2722 (2000).
[38] H. M. Wiseman, Phys. Rev. A **49**, 2133 (1994).
[39] W. K. Wooters and W. H. Zurek, Nature (London) **299**, 802 (1982).